

**DYNAMICS OF THE CAVITATION CLOUD IN SUBMERGED
WATERJET AND ITS RELATION WITH JET EROSION INTENSITY**

C. Peng, G.S. Li, S.C. Tian
China University of Petroleum, Beijing
Beijing, China

ABSTRACT

There is obvious cavitation in our high-pressure submerged waterjet which is originally used for cutting metals and rocks. To understand the effect of cavitation on jet erosion, the dynamic change of cavitation cloud in waterjet was visualized through high-speed photography, which was further processed using Proper Orthogonal Decomposition (POD). The results are analyzed together with the erosion experiment of aluminum samples under various standoff distances. It is found that along with the waterjet impingement, cavitation also attributes to the erosion of aluminum sample. Under small standoff distance which is usually applied for cutting, the effect of cavitation is negligible while the high-speed waterjet is the dominant contributor of erosion. With the increasing of standoff distance, cavitation erosion becomes more significant while the intensity of waterjet attenuates. Cavitation erosion is closely related to the dynamics of cavitation cloud that are illustrated in POD modes. The erosion pattern and mass loss of sample both change with stand-off distance. The role of cavitation in submerged waterjet erosion is clarified. Besides, we provide a possible extra application of conventional waterjet cutting system. It can be used to generate cavitation waterjet with little adjustment.

1. INTRODUCTION

Submerged waterjet is a widely-used technology of cold cutting. As the standoff distance increases, jet potential core narrows and the cutting capacity of waterjet sharply attenuates. At the same time, jet shear layer expands, providing turbulent pressure that can induce massive cavitation. Cavitation refers to the phenomenon characterized by vapor generation and condensation in liquids. It frequently occurs in hydraulic devices such as rotating machinery and injectors. In most cases it is unwelcome because cavitation will lead to vibration, low efficiency, noise, and erosion (Dular and Coutier-Delgosha). As a result of cavitation in submerged waterjet, there should be two peaks of erosion rates with increasing standoff distance (Momma and Lichtarowicz; Yamauchi et al.; Soyama and Lichtarowicz). The first peak is attributed to waterjet erosion while the second one is attributed to cavitation bubbles collapse.

Submerged cavitation waterjet (SCWJ), which operates around the second erosion peak, has been successfully used for shotless peening (Soyama, Saito and Saka; Soyama, Kikuchi, et al.), petroleum drilling (Johnson et al.; Gensheng et al.), disposing of organic waste water (Kalumuck and Chahine), etc.. Since the damage of SCWJ is caused by cavitation bubbles, it is highly desired to find the link between the behavior of cavitation cloud and the erosion capability. So far several pioneering works have been done. Optical observation of cavitation structures above hydrofoils was conducted and an obvious correlation between cavitation structures and cavitation erosion was found (Dular et al.). The position and distribution of pits on hydrofoil surface correlate to the distribution of the images' standard deviation of grey level. Moreover, there were other attempts to relate the distribution of cavitation bubbles to the erosion pattern of test sample (Petkovšek and Dular; Hutli et al.; R Watanabe et al.). The scope of cavitation bubble collapse at sample surface was found to match the ring-shape erosion pits very well. However, all of previous works only used a couple of images to represent the cavitation erosion process, which we think is defective since periodic cavitation events typically have a frequency of several thousands Hz and behave not exactly the same in different cycles. To have a better knowledge about the dynamics of cavitation cloud and its relation to cavitation erosion, it is necessary to investigate cavitation events from a statistical point of view.

To visualize the cavitation cloud in SCWJ, high-speed photography seems to be the most popular method. It was firstly adopted by Chahine et al. (Chahine, Kalumuck, et al.; Chahine, Johnson Jr, et al.), who found that there was periodic shedding of cavitation cloud in SCWJ.. Hydraulic conditions such as upstream pressure and cavitation number would affect the size and shedding frequency of cavitation cloud. Soyama et al. (Soyama, Yamauchi, et al.) observed that the shedding frequency of cavitation cloud decreases, while the maximum length increases, with increasing upstream pressure. Hutli et al. (Hutli and Nedeljkovic) calculated the shedding frequency under different upstream pressure and nozzle geometry using high-speed photography images. Nishimura et al. (Nishimura, Takakuwa and Soyama) established the similarity law between shedding frequency and hydraulic parameters. Vortex shedding was proposed as the reason for the periodic shedding of cavitation cloud. Wright et al. (Wright et

al.) investigated the size, width, length, and shedding frequency of cavitation cloud under different Reynolds numbers. Sato and cooperators (Saito and Sato; Sato, Takahashi and Sugimoto) utilized frame difference method to analyzes the shedding, transition and collapse process of cavitation cloud using horn-type nozzle.

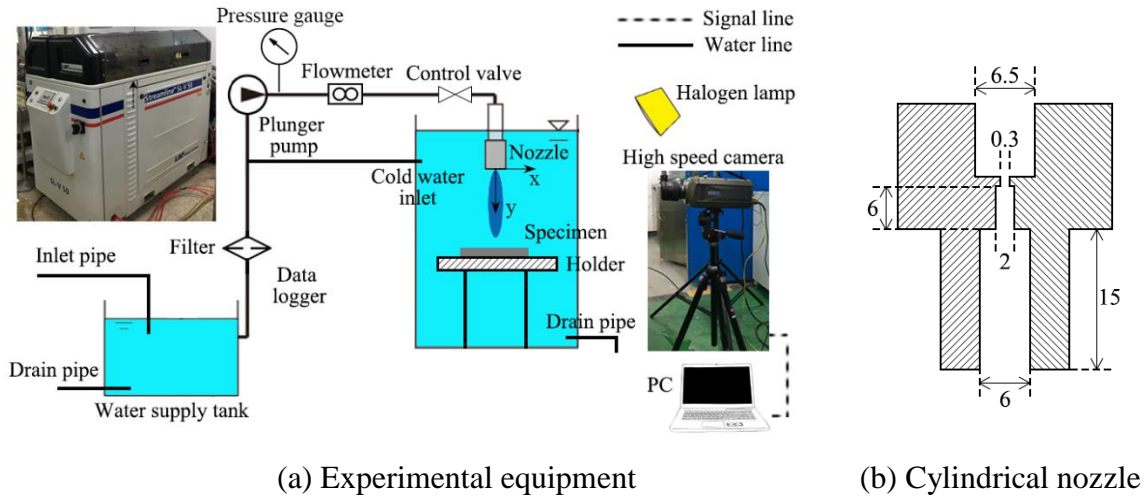
In this paper, we are going to use POD (proper orthogonal decomposition) to analyze the high-speed photography images. POD is an efficient method to identify spatial and temporal coherent structures in flow fields. It decomposes a time series of vector or scalar field into a set of basic spatial modes and temporal coefficients (Holmes, Lumley and Berkooz). POD was firstly adopted to study turbulent flow by Lumley (Lumley). Large scale structures and main patterns of the field can be highlighted in POD modes. Besides, the coefficients contain temporal information about the whole flow process. Recently POD was introduced to the study of cavitation flow (Danlos et al.; Tomov et al.; Ryuta Watanabe et al.; Prothin, Billard and Djeridi; Utturkar, Zhang and Shyy). Utturkar et al. (Utturkar, Zhang and Shyy) applied POD to characterize the differences between cavitation models. Danlos et al. (Danlos et al.) proposed to use contribution fraction of the second POD mode to distinguish different cavitation regimes in a convergent-divergent nozzle. Watanabe et al. (Ryuta Watanabe et al.) calculated the spatial modes of cavitation cloud in SCWJ. The weighting coefficients that contain temporal information about SCWJ, were found to be very useful to explore the frequency feature of transient cavitation flow (Danlos et al.; Zhang, Xu and Li).

This paper is going to address the transition of waterjet to SCWJ with increasing standoff distance, and analyze the relation between erosion intensity and the dynamics of cavitation cloud in SCWJ. Hopefully present work will improve the physical understanding of the cavitation phenomenon and cavitation damage.

2. MATERIAL AND METHODS

2.1 Experimental setup

The combined experiments of high-speed visualization and erosion test were carried out at the same time. The test rig is schematically depicted in **Figure 1 (a)**. A high-pressure plunger pump (KMT Streamline SL-V50) provided the pressure to generate SCWJ. The upstream pressure was read from a pressure gauge (accuracy $\pm 0.3\%$ FS). A turbine flowmeter (accuracy $\pm 0.5\%$ FS) was used to measure the flow rate. A cylindrical nozzle (**Figure 1 (b)**) was used, with throat diameter being 0.3 mm. A water vessel made of transparent acrylic resin was used to produce submerge condition. Tap water was used and additional cold water was injected to the vessel to maintain water temperature, which was kept around 22 °C during the experiments. The lateral and axial coordinates x and y were defined, with the origin set at the nozzle exit. Standoff distance y can be adjusted at a resolution of 0.1 mm.



(a) Experimental equipment

(b) Cylindrical nozzle

Figure 1. Experimental setup

A high-speed camera (Phantom V310) was used to visualize the cavitation cloud, operating at a frame rate of 20,000 fps. Maximum image size was 128×504 pixels. Illumination was provided by a halogen lamp, placed right above the camera. Original high-speed photos were clipped and processed into gray-scale images using commercial software. The specimen used for erosion test was pure aluminum plate (Chinese Standard 1060). The diameter was 100 mm while the height was 8 mm (**Figure 2**). The surface was deliberately polished and the surface roughness Ra was less than $1 \mu\text{m}$. For erosion test and high-speed photography of cavitation cloud, 6 standoff distances were investigated (1, 2, 3, 4, 5 and 6 cm), with upstream pressure fixed at 50 MPa. The flow rate was 0.96 L/min. Nozzle discharge coefficient was 0.71. The water in supply tank was prepared a day before experiment and exposed to atmosphere for 24 hr. After each test, the specimen was dried and then weighted by an electronic balance (resolution 0.1 mg). Each data point of mass loss was the average of three repetition experiments.

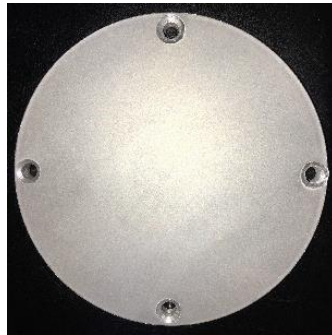


Figure 2. Polished aluminum plate

2.2 Principle of Proper Orthogonal Decomposition (POD)

POD is essentially a linear approximation method which disintegrates transient vector field or scalar field into the sum of a series of orthonormal basis functions (modes), ϕ_m and corresponding weighting coefficients (Chatterjee; Chen, Reuss and Sick). Modes contain spatial information while weighting coefficients contain temporal information about the field. Field at a specific time is called a 'snapshot' and the number of modes is equal to the number of snapshots. In this paper, the number of snapshots is 2000, and the snapshot method proposed

by (Sirovich) is used. Each gray image of cavitation cloud can be regarded as a snapshot (gray level field), G (Prothin, Billard and Djeridi). The aim is to decompose all K snapshots $G(k)$ into a linear combination of M modes φ_m and $K \times M$ weighting coefficients $c_m^{(k)}$:

$$G^{(k)} = \sum_{m=1}^M c_m^{(k)} \varphi_m \quad (1)$$

The process is as follows:

Firstly, representing the gray levels of every pixels in all K snapshots with a $K \times (I \cdot J)$ matrix U :

$$U = \begin{bmatrix} u_{i=1,j=1}^{(1)} & u_{i=1,j=2}^{(1)} & \cdots & u_{i=1,j=J}^{(1)} & u_{i=2,j=1}^{(1)} & u_{i=2,j=2}^{(1)} & \cdots & u_{i=I,j=J}^{(1)} \\ u_{i=1,j=1}^{(2)} & u_{i=1,j=2}^{(2)} & \cdots & u_{i=1,j=J}^{(2)} & u_{i=2,j=1}^{(2)} & u_{i=2,j=2}^{(2)} & \cdots & u_{i=I,j=J}^{(2)} \\ \cdots & \cdots & \cdots & \cdots & \cdots & \cdots & \cdots & \cdots \\ u_{i=1,j=1}^{(k)} & u_{i=1,j=2}^{(k)} & \cdots & u_{i=1,j=J}^{(k)} & u_{i=2,j=1}^{(k)} & u_{i=2,j=2}^{(k)} & \cdots & u_{i=I,j=J}^{(k)} \\ \cdots & \cdots & \cdots & \cdots & \cdots & \cdots & \cdots & \cdots \\ u_{i=1,j=1}^{(K)} & u_{i=1,j=2}^{(K)} & \cdots & u_{i=1,j=J}^{(K)} & u_{i=2,j=1}^{(K)} & u_{i=2,j=2}^{(K)} & \cdots & u_{i=I,j=J}^{(K)} \end{bmatrix} \quad (2)$$

where i and j indicate the position of the pixel; k means k th snapshot; I is image length in pixels, J is image width in pixels.

The spatial correlation matrix W is:

$$W = \frac{1}{K} U U^T \quad (3)$$

The key of POD is to find a sequence of orthonormal modes that reflect the basic structures of the dynamic field, which are determined by solving following equations:

$$\begin{cases} \sum_{k=1}^K \left\| G^{(k)} - \sum_{m=1}^M c_m^{(k)} \varphi_m \right\|_F \rightarrow \min \\ (\varphi_i, \varphi_j) = \delta_{ij} = \begin{cases} 0 & i = j \\ 1 & i \neq j \end{cases} \end{cases} \quad (4)$$

where $\| \cdot \|_F$ is Frobenius norm.

Modes embody the basic compositions of the field. Snapshots can be reconstructed through equation (1), i.e., summing the products of every mode and corresponding coefficients. Here, modes of gray level field illustrate the fundamental compositions of cavitation cloud. In particular, if the flow process is dominated by a periodic behavior, as in the present study, low-order modes should be organized in pairs, which represent of the same orthogonal component of the periodic phenomenon (Graftieaux, Michard and Grosjean).

The weighting coefficients are computed by projecting the original snapshots onto modes,

presented as a matrix:

$$C = \begin{bmatrix} c_1^{(1)} & c_2^{(1)} & \dots & c_M^{(1)} \\ c_1^{(2)} & c_2^{(2)} & \dots & c_M^{(2)} \\ \dots & \dots & \dots & \dots \\ c_1^{(K)} & c_2^{(K)} & \dots & c_M^{(K)} \end{bmatrix} \quad (6)$$

c_m^k represents the contribution of m th mode to the reconstruction of k th snapshot; $K=M$. In velocity field, $0.5(c_m^k)^2$ is the energy contributed by the m th mode to k th snapshot, while $KE_m = 0.5 \sum_{k=1}^K (c_m^k)^2$ can be interpreted as the kinetic energy per unit mass included in the m th mode (Berkooz, Holmes and Lumley; Chatterjee). The ‘energy fraction’ ke_m is defined as:

$$ke_m = KE_m / \sum_{m=1}^M KE_m \quad (7)$$

which reflects the degree of contribution of each mode to the reconstruction of all snapshots. Modes are arranged with decreasing energy fraction. In present gray level field, energy fractions of modes represent their degree of contribution to the reconstruction of cavitation cloud snapshots. Low-order modes are the dominant compositions of cavitation cloud gray filed.

3. RESULTS AND DISCUSSION

3.1 Periodic behavior of cavitation cloud in SCWJ

As shown in **Figure 3**, a typical cycle of cavitation cloud in SCWJ contains inception, development, shedding and collapse phases (Soyama; R Watanabe et al.). Set the first image as the moment of 0 ms. The interval between two adjacent images is 0.1 ms. At around 0 ms, a new cloud is initialed at the nozzle exit (cavitation cloud inception), while the former cavitation cloud near the specimen has totally collapsed and disappeared. The new cloud grows and rapidly moves downstream, beginning to contact specimen at around 0.4 ms. When a single cavitation bubble reaches the specimen surface, the stagnation pressure will lead to the collapse of bubble, which shall induce microjet and shock wave that finally cause the erosion of the specimen. The continuous destructive collapse of massive coalesce of cavitation bubbles are observable from 0.5 to 1.0 ms. Cavitation cloud shedding occurs at about 0.9 ms. The unsteady behavior of cavitation cloud is thought to be closely related to the complex pressure gradient and coherent structures in jet shear layer. This can be justified by the fan-shaped bumps occurring at the sides of SCWJ, mostly visible at 8 ms. Compared with the situation without specimen, a major difference is that the collapse of cavitation cloud may happen before shedding under small standoff distance. This is because of the faster pressure recover resulting from the existence of specimen.

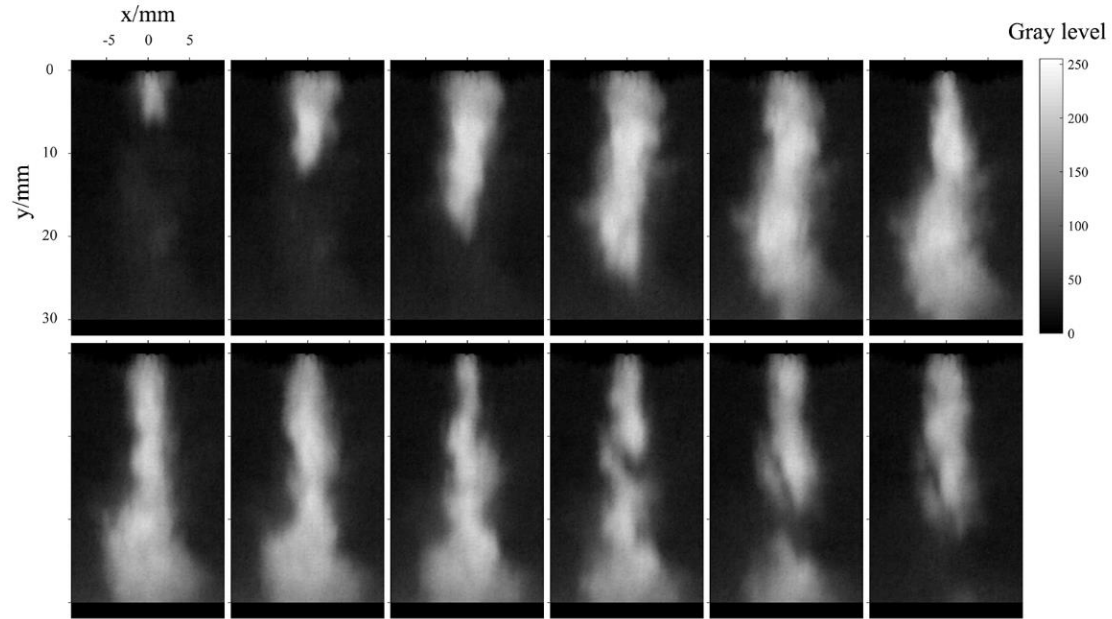


Figure 3. Periodic behavior of cavitation cloud (standoff distance=30 mm)

3.2 POD results

The first 4 POD modes and their energy fractions at standoff distance 1, 3 and 5 cm are shown in **Figure 4**. In general, the 1st modes are very close to the ensemble-average gray level fields and they are the most important components of cavitation cloud gray field, with energy fraction larger than 80%. It is interesting to find that the shape of mode 1 is very similar to potential core of waterjet, suggesting the close relation between cavitation cloud and high-speed potential core. As mentioned before, that low-order modes 2~4 are organized in pairs is the evidence of prominent periodic behavior of the cavitation cloud in SCWJ. The 2nd modes comprise two counter-rotating lobe-structures that are characteristic of spatial periodic shedding. The 3rd modes represent the same structures with a delay to downstream direction, which is a classical feature of cavitation shedding (Prothin, Billard and Djeridi).

When standoff distance is 1 cm, mode 1 shows the direct contact of cavitation cloud with the specimen. Besides, mode 2~4 also show the massive distribution of cavitation cloud at specimen surface. As the standoff distance increases, cavitation cloud cannot reach specimen in mode 1 and the mode that captures the extensive contact between cavitation cloud and specimen gradually shifts to higher order (3rd mode under 3 cm standoff distance, 5th mode under 5 cm standoff distance (not shown)). In this way, if we only predict cavitation erosion intensity based on POD modes, it may lead to an elusive conclusion that cavitation erosion should decrease with increasing standoff distance. However, as demonstrated by the erosion test below, this is not the truth.

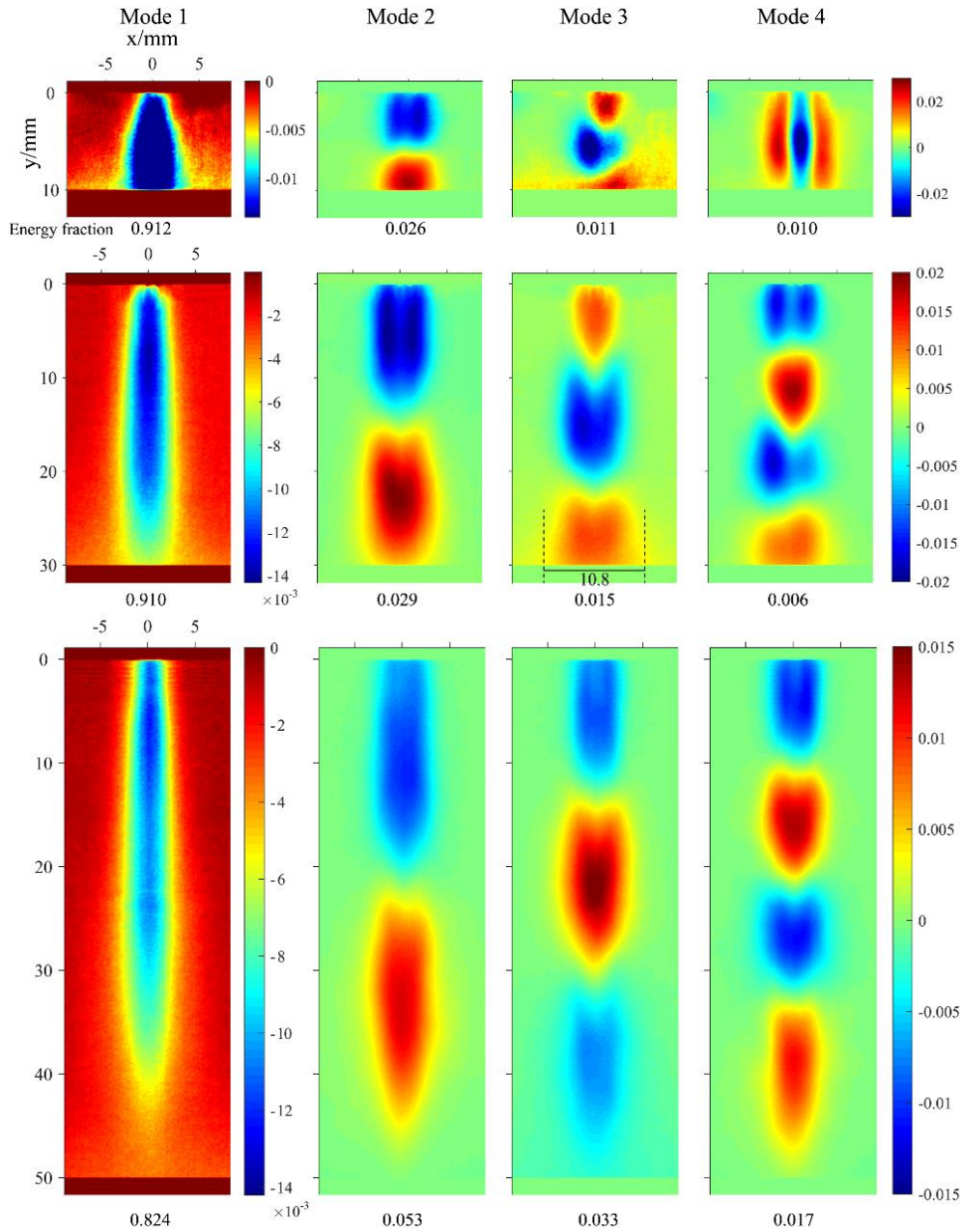


Figure 4. First 4 POD modes and energy fractions (standoff distance 1, 3 and 5 cm)

3.3 Erosion patterns and mass loss

The macroscopic appearance of eroded specimen under different standoff distances and exposure times are presented in **Figure 5**. The change of erosion patterns can be observed. At 1 cm standoff distance, the central pit eroded by waterjet accounts for almost all the mass loss of specimen while the effect of cavitation is negligible in terms of mass loss. It is deemed that cavitation bubbles does not have enough time to grow and reach their maximum size before reaching specimen at small standoff distance. So the erosion ability of single cavitation bubble is weak and the ultimate cavitation damage is trivial. However, cavitation around the waterjet potential core does change the surface morphology around central pit, in the form of permanent plastic deformation. As the standoff distance increases, the erosion ability of central waterjet

steeply attenuates. At 3 cm standoff distance, the central pit is much shallower and smaller compared with that at 1 cm standoff distance. On the other hand, cavitation erosion, in the shape of a large number of hemispheric pits, is remarkable and responsible for most of the mass loss. It is noted that some of the cavitation pits exceed the central pit in both depth and diameter. A classic ring-shape distribution of cavitation pits is obtained, which supports the idea that cavitation bubbles mainly reside in the shear layer. An undamaged zone exists between the cavitation ring and central pit. As standoff distance further increases, cavitation erosion intensity decreases. At 5 cm standoff distance, both the central pit and cavitation pits are less evident. Moreover, the undamaged zone disappears because of the full development of shear layer in jet transverse direction.

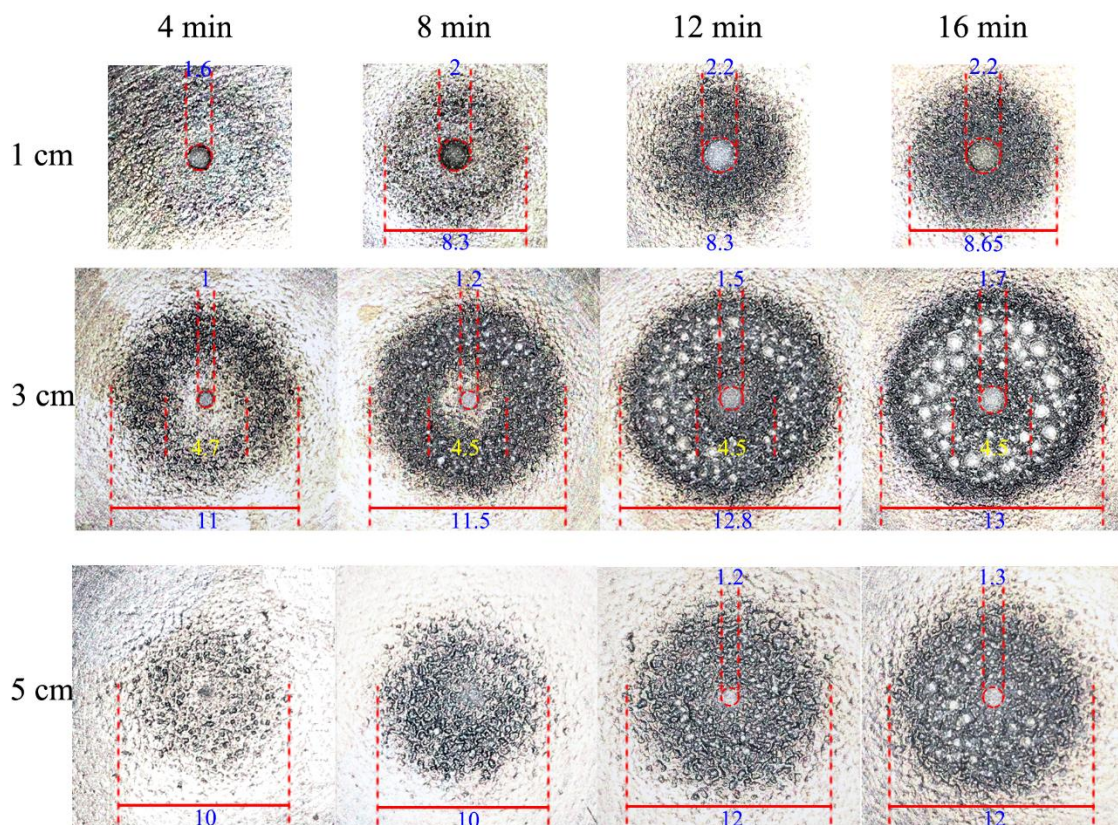


Figure 5. Eroded specimen (dimension unit: mm)

Comparing **Figure 4** and **Figure 5**, it is found that the attenuation of cavitation erosion at larger standoff distance (5 cm) should be attributed to the fact that less cavitation bubbles are able to reach the specimen, which is clearly depicted in modes 1~4. At small standoff distance (1 cm), on contrary, although a lot of cavitation bubbles reach and collapse at specimen surface, they are rudimentary and not capable of causing obvious damage. This proves that the visualization method alone can only capture the distribution of cavitation cloud but fails to predict the cavitation erosion intensity. Nevertheless, a close correlation between total mass loss and the energy fraction of mode 1 is established (**Figure 6**). As standoff distance increases, the total mass loss falls from the first peak, rises to a second peak and finally falls again. The energy fraction of mode 1 has the same trend and it is possible to use this parameter as an indicator to find the optimal standoff distance for cavitation erosion.

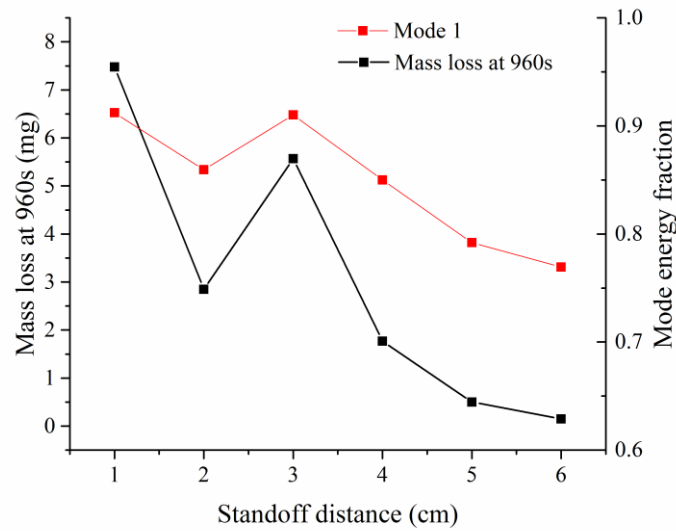


Figure 6. Mass loss of specimen and 1st mode energy fraction

4. CONCLUSIONS

In present study, the erosion ability of submerged cavitation water jet is successfully related to the dynamics of cavitation cloud by joint erosion test and high-speed visualization. Several conclusions can be drawn:

1. An extended application of conventional waterjet cutting system was achieved. It can be used to generate cavitation jet with almost no adjustment. A typical cycle of cavitation cloud in SCWJ contains inception, development, shedding and collapse phases. Due to the existence of specimen, static pressure recovers faster and the collapse of cavitation cloud may happen before shedding when standoff distance is small.
2. Low-order POD modes are organized in pairs, which verifies the periodic behavior of the cavitation cloud in SCWJ. As standoff distance increases, the mode that captures the extensive contact between cavitation cloud and specimen gradually shifts to higher-order modes.
3. Damage pattern of aluminum specimen is closely related to standoff distance. Under small standoff distance, cavitation erosion is negligible while the high-speed waterjet is the dominant contributor for mass loss. With increasing standoff distance, cavitation erosion rises and then falls while the erosion of waterjet monotonically attenuates. Typical ring-shape distribution of cavitation pits is obtained at proper standoff distance.
4. Although cavitation erosion is closely related to the dynamics of cavitation cloud, POD modes can only capture the distribution of cavitation cloud but fail to predict the cavitation erosion intensity. However, the energy fraction of mode 1 has the same trend as mass loss along standoff distance. Thus it is possible to use the 1st mode energy fraction as an indicator to determine the optimal standoff distance for SCWJ.

5. ACKNOWLEDGMENTS

We are sincerely grateful for the financial support of National Natural Science Foundation of China (grant number, U1562212) and Chinese Ministry of Science and Technology (grant number, 2016YFE0124600).

6. REFERENCES

- Berkooz, Gal, Philip Holmes, and John L Lumley. "The Proper Orthogonal Decomposition in the Analysis of Turbulent Flows." *Annual review of fluid mechanics* 25.1 (1993): 539-75. Print.
- Chahine, GL, et al. *Internal and External Acoustics and Large Structures Dynamics of Cavitating Self-Resonating Water Jets*: Sandia National Labs., Albuquerque, NM (USA); Tracor Hydronautics, Inc., Laurel, MD (USA), 1987. Print.
- Visualization Study of Structured Cavitating Jets*. ASME Fluid Engineering Division Cavitation and Multiphase Flow Forum, Cincinnati, OH. 1987. Print.
- Chatterjee, Anindya. "An Introduction to the Proper Orthogonal Decomposition." *Current science* 78.7 (2000): 808-17. Print.
- Chen, Hao, David L Reuss, and Volker Sick. "On the Use and Interpretation of Proper Orthogonal Decomposition of in-Cylinder Engine Flows." *Measurement Science and Technology* 23.8 (2012): 085302. Print.
- Danlos, Amélie, et al. "Cavitation Regime Detection through Proper Orthogonal Decomposition: Dynamics Analysis of the Sheet Cavity on a Grooved Convergent–Divergent Nozzle." *International Journal of Heat and Fluid Flow* 47 (2014): 9-20. Print.
- Dular, Matevž, et al. "Relationship between Cavitation Structures and Cavitation Damage." *Wear* 257.11 (2004): 1176-84. Print.
- Dular, Matevž, and Olivier Coutier-Delgosha. "Thermodynamic Effects During Growth and Collapse of a Single Cavitation Bubble." *J. Fluid Mech* 736 (2013): 44-66. Print.
- Gensheng, Li, et al. "Investigation and Application of Self-Resonating Cavitating Water Jet in Petroleum Engineering." *Petroleum science and technology* 23.1 (2005): 1-15. Print.
- Graftieaux, Laurent, Marc Michard, and Nathalie Grosjean. "Combining Piv, Pod and Vortex Identification Algorithms for the Study of Unsteady Turbulent Swirling Flows." *Measurement Science and Technology* 12.9 (2001): 1422. Print.
- Holmes, Philip, John L Lumley, and Gal Berkooz. *Turbulence, Coherent Structures, Dynamical Systems and Symmetry*. Cambridge university press, 1998. Print.
- Hutli, Ezddin AF, and Milos S Nedeljkovic. "Frequency in Shedding/Discharging Cavitation Clouds Determined by Visualization of a Submerged Cavitating Jet." *Journal of Fluids Engineering* 130.2 (2008): 021304. Print.
- Hutli, Ezddin, et al. "The Relation between the High Speed Submerged Cavitating Jet Behaviour and the Cavitation Erosion Process." *International Journal of Multiphase Flow* 83 (2016): 27-38. Print.
- Johnson, VE, et al. "Cavitating and Structured Jets for Mechanical Bits to Increase Drilling Rate—Part II: Experimental Results." *Journal of energy resources technology* 106.2 (1984): 289-94. Print.

- Kalumuck, Kenneth M, and Georges L Chahine. "The Use of Cavitating Jets to Oxidize Organic Compounds in Water." *Journal of Fluids Engineering* 122.3 (2000): 465-70. Print.
- Lumley, John Leask. "The Structure of Inhomogeneous Turbulent Flows." *Atmospheric turbulence and radio wave propagation* (1967): 166-78. Print.
- Momma, T, and A Lichtarowicz. "A Study of Pressures and Erosion Produced by Collapsing Cavitation." *Wear* 186 (1995): 425-36. Print.
- Nishimura, Satoshi, Osamu Takakuwa, and Hitoshi Soyama. "Similarity Law on Shedding Frequency of Cavitation Cloud Induced by a Cavitating Jet." *Journal of Fluid Science and Technology* 7.3 (2012): 405-20. Print.
- Petkovšek, Martin, and Matevž Dular. "Simultaneous Observation of Cavitation Structures and Cavitation Erosion." *Wear* 300.1 (2013): 55-64. Print.
- Prothin, Sebastien, Jean-Yves Billard, and Henda Djeridi. "Image Processing Using Proper Orthogonal and Dynamic Mode Decompositions for the Study of Cavitation Developing on a Naca0015 Foil." *Experiments in fluids* 57.10 (2016): 157. Print.
- Instantaneous Behavior of Cavitation Clouds at Impingement of Cavitating Water-Jet*. Sixth International Symposium on Cavitation (CAV2006). 2006. Print.
- Effects of Diffuser Length on Cloud Cavitation in an Axisymmetrical Convergent-Divergent Nozzle*. ASME/JSME/KSME 2015 Joint Fluids Engineering Conference. 2015. American Society of Mechanical Engineers. Print.
- Sirovich, Lawrence. "Turbulence and the Dynamics of Coherent Structures Part I: Coherent Structures." *Quarterly of applied mathematics* 45.3 (1987): 561-71. Print.
- Soyama, H, and A Lichtarowicz. "Useful Correlations for Cavitating Water Jet." *The Review of High Pressure Science and Technology* 7 (1998): 1456-58. Print.
- Soyama, Hitoshi. "High-Speed Observation of a Cavitating Jet in Air." *Journal of Fluids Engineering* 127.6 (2005): 1095-101. Print.
- Soyama, Hitoshi, et al. "Introduction of Compressive Residual Stress into Stainless Steel by Employing a Cavitating Jet in Air." *Surface and Coatings Technology* 205.10 (2011): 3167-74. Print.
- Soyama, Hitoshi, Kenichi Saito, and Masumi Saka. "Improvement of Fatigue Strength of Aluminum Alloy by Cavitation Shotless Peening." *Journal of engineering materials and technology* 124.2 (2002): 135-39. Print.
- Soyama, Hitoshi, et al. "High-Speed Observations of the Cavitation Cloud around a High-Speed Submerged Water Jet." *JSME International Journal Series B Fluids and Thermal Engineering* 38.2 (1995): 245-51. Print.
- Pod Study of Aerated Cavitation in a Venturi Nozzle*. Journal of Physics: Conference Series. 2015. IOP Publishing. Print.
- Utturkar, Yogen, Baoning Zhang, and Wei Shyy. "Reduced-Order Description of Fluid Flow with Moving Boundaries by Proper Orthogonal Decomposition." *International Journal of Heat and Fluid Flow* 26.2 (2005): 276-88. Print.
- Watanabe, R, et al. "Simultaneous Shadowgraph Imaging and Acceleration Pulse Measurement of Cavitating Jet." *Wear* 358 (2016): 72-79. Print.
- Watanabe, Ryuta, et al. "Shadowgraph Imaging of Cavitating Jet." *Journal of Flow Control, Measurement & Visualization* 3.03 (2015): 106. Print.

- Wright, Michael M, et al. "Cavitation of a Submerged Jet." *Experiments in fluids* 54.6 (2013): 1-21. Print.
- Yamauchi, Yoshiaki, et al. "Suitable Region of High-Speed Submerged Water Jets for Cutting and Peening." *JSME International Journal Series B Fluids and Thermal Engineering* 38.1 (1995): 31-38. Print.
- Applicability of Principle Components Analysis (Pca) to Evaluate the Dynamic Characteristics of Cavitation from Captured Images.* Fluid Power and Mechatronics (FPM), 2015 International Conference on. 2015. IEEE. Print.

7. NOMENCLATURE

- POD – proper orthogonal decomposition
 SCWJ – submerged cavitation waterjet
 i – x position of the pixel
 j – y position of the pixel
 k – the sequence of the snapshot
 x – radial position, mm
 y – standoff distance, mm
 G – gray level field (snapshot of cavitation cloud)
 K – the number of snapshots
 M – the number of modes
 W – spatial correlation matrix
 I – image length in pixels
 J – image width in pixels
 Ra – surface roughness, μm
 φ_m – basic functions of POD
 $c_m^{(k)}$ – weighting coefficient of m th mode toward k th snapshot
 ke_m – energy fraction of the m th mode
 KE_m – the kinetic energy per unit mass included in the m th mode